JSR Publications

Available Online

J. Sci. Res. **12** (1), 111-133 (2020)

JOURNAL OF SCIENTIFIC RESEARCH

www.banglajol.info/index.php/JSR

DNA and BSA Interaction, DNA Cleavage and *In Vitro* Cytotoxicity of Copper(II) Complexes: [Cu(bba)(phen)]$(ClO_4)_2$ is Promising Chemotherapeutic Scaffold

J. Manivel[1], S. Sangeetha[1,2], M. Murali[1*]

[1]Coordination and Bioinorganic Chemistry Research Laboratory, Department of Chemistry National College (Autonomous), Tiruchirappalli 620 001Tamil Nadu, India

[2]Department of Chemistry, Tamilavel Umamaheswaranar Karanthai Arts College, Thanjavur 613 002 Tamil Nadu, India

Received 22 August 2019, accepted in final revised form 18 November 2019

Abstract

Three mononuclear copper(II) complexes of the type [Cu(bba)(bpy/phen/dpa)]$(ClO_4)_2$ (**1**-**3**), where bba (*N*,*N*-bis(benzimidazol-2-ylmethyl)amine) and bpy (2,2'-bipyridine, **1**) or phen (1,10-phenanthroline, **2**) or dpa (2,2'-dipyridylamine, **3**), have been isolated. The coordination geometry of **1** around copper(II) is square pyramidal. The electronic absorption (639-667 nm) and EPR spectral parameters ($g_{\|}$, ~2.25; $A_{\|}$, 181-186 × 10^{-4} cm^{-1}; $g_{\|}/A_{\|}$, 122−134 cm) reveal that **1**-**3** possesses a square pyramidal geometry with CuN_5 chromophore. Different spectral and electrochemical measurements clearly demonstrate partial intercalative interaction of **1**-**3** to CT DNA. Complexes strongly quench the intrinsic fluorescence of BSA through a static quenching procedure by forming BSA-(**1**/**2**/**3**) adducts, which are stabilized by hydrophobic interactions. The number of binding sites and binding constants were calculated. The energy transfer from BSA to Cu(II) complexes occurs with high probability. Notably, **1**-**3** exhibit more effective pUC 19 DNA cleavage in the presence of H_2O_2. Complexes **2** and **1** show remarkable cytotoxicity (IC_{50}: **2**, 2.17; **1**, 8.33 μM) against human cervical carcinoma cells (HeLa) and more potent than cisplatin (IC_{50}, 16.40 μM) while **3** exhibits less cytotoxicity (IC_{50}, 20.82 μM). The DNA binding propensity, cleavage ability and cytotoxicity follow the order **2**>**1**>**3**. Interestingly, they are non-toxic to healthy cells.

Keywords: Copper(II) complexes; Partial intercalation; Static quenching; DNA cleavage; Cytotoxicity.

doi: http://dx.doi.org/10.3329/jsr.v12i1.42745 J. Sci. Res. **12** (1), 111-133 (2020)

1. Introduction

The serendipitous discovery of cisplatin [1] has revolutionized the cancer treatment; however, side-effects associated with the drug restrict its wider use [2]. Copper(II) complexes are regarded as promising and have attracted considerable attention owing to their capability of interacting directly with DNA and BSA [3,4]. Many studies reveal that

*Corresponding author: ma66mu@gmail.com

DNA is the primary intracellular target of anticancer drugs, since the interaction between small molecules and DNA able to cause DNA damage, block DNA synthesis in cancer cells [5-8]. Therefore, under physiological conditions, metal complexes that possess efficient DNA binding and cleavage are regarded as potential candidates for use as therapeutic agents in medicinal applications and for genomic research [9-12]. On the other hand, a vast majority of cytotoxic metal-containing compounds are administered intravenously, special consideration should be given to interactions of the metal drug with macromolecular blood components, which can then be taken up by and accumulate in tumor tissue. In this context, binding toward serum proteins, like albumin or transferrin that may perform a transport function for a metal. Such interactions determine the overall drug distribution and excretion and differences in efficacy, activity, and toxicity [13,14].

Benzimidazole moiety is structurally related to purine bases and is found in a variety of naturally occurring compounds such as vitamin B_{12}. Benzimidazole derivatives display a wide variety of pharmacological properties including antitumor activity [15] and inhibition of nucleic acid synthesis [16]. Transition metal complexes consist of benzimidazole ligands act as cytotoxic [17,18], antiviral [18] and antiamoebic [19] agents. Moreover, ruthenium(I) [20] and zinc(II) [21] complexes of 2,6-bis(benzimidazol-2-yl)pyridine have DNA cleaving properties. Copper(II) complexes with benzimidazole-derived bidentate chelating ligands show most active cytotoxic activity [22] with different human tumor cell lines. There are also many examples in the literature of copper complexes of ligands containing α-diimino (-N=C-C=N-) moiety such as phenanthroline that can induce apoptosis [23] and 2-(4'-thiazolyl)benzimidazole that display antimicrobial activity [24]. In particular, the non-planar nature of benzimidazole ligands, their flexibility, and bulkiness affect the kinetics and cytotoxic properties of the corresponding metal complexes. In addition, benzimidazole-based ligands can possess N-H moiety which can facilitate DNA cleavage in cancer cells [25].

Thus, we have synthesized a series of mixed-ligand copper(II) complexes of the type $[Cu(bba)(diimine)](ClO_4)_2$ [where bba is *N*,*N*-bis(benzimidazol-2-ylmethyl)amine and diimine is 2,2'-bipyridine (**1**, bpy) or 1,10-phenanthroline (**2**, phen) or 2,2'-dipyridylamine (**3**, dpa)] and investigated their interaction with calf thymus (CT) DNA and bovine serum albumin (BSA), DNA cleavage activity and *in vitro* cytotoxic properties against human cervical carcinoma cell line (HeLa) and normal mouse embryonic fibroblasts cell line (NIH 3T3).

2. Materials and Methods

Copper(II) perchlorate hexahydrate (Sigma Aldrich), 2,2′-bipyridine, 1,10-phenanthroline (Merck), 2,2'-dipyridylamine (Sigma Aldrich) and *Tetra*-*N*-butylammonium bromide (Thomas Baker) were used as received. The commercial solvents were distilled and then used for the preparation of ligand and complexes. The ligand *N*,*N*-bis(benzimidazol-2-ylmethyl)amine (bba) was synthesized according to the published procedure [26,27]. Calf thymus (CT) DNA and bovine serum albumin (BSA) were purchased from Sigma Aldrich and stored at -20 °C. Ultrapure MilliQ water (18.2 mΩ) was used for all the experiments.

The elemental analyses (C, H, N) were carried out using a Perkin-Elmer 2400 series II analyzer. The electrical conductivity was obtained with a Systronic 305 conductivity bridge, using 1×10^{-3} M solution of the complex in dimethylformamide (DMF). Finnigan MAT TSQ-700 equipped with a custom-made electrospray interface (ESI) was used to perform mass spectrometry experiments. Spectra were collected by constant fusion of the analyte dissolved in DMF. Magnetic susceptibility value at 298 K was obtained using Model 300 Lewis-coil-force magnetometer of George Associate Inc. (Berkley, USA) make. The electronic spectra were recorded using Perkin-Elmer Lambda 35 UV-Visible spectrophotometer. The room temperature (RT) solid and liquid-nitrogen temperature (LNT) DMF solution electron paramagnetic resonance spectra were obtained on a JEOL JES-FA200 ESR spectrometer. All fluorescence measurements were performed using a Shimadzu RF-5301PC spectrofluorophotometer equipped with a thermostatic bath and a 10 mm quartz cuvette. The pH was potentiometrically measured using an Elico LI 120 pH meter equipped with a combined glass electrode. Cyclic voltammetry (CV) and differential pulse voltammetry (DPV) on glassy carbon disc electrode were performed in a CHI 620C electrochemical analyzer at 27 ± 0.5 °C. The working electrode was a glassy carbon disk (0.0707 cm^2), the reference electrode a saturated calomel electrode and the counter electrode a platinum wire. In DMF solution 0.1 M Tetra-*N*-butylammonium perchlorate and in buffer solution (pH 7.1) 2% DMF - 5 mMTris-HCl/50 mMNaCl buffer was used as supporting electrolytes. Solutions were deoxygenated by purging with nitrogen gas for 15 min prior to measurements; during measurements, a stream of N_2 gas was passed over them. The redox potential $E_{1/2}$ was calculated from the anodic (E_{pa}) and cathodic (E_{pc}) peak potentials of CV traces as $(E_{pa} + E_{pc})/2$ and as $E_p + \Delta E/2$ (ΔE is the pulse height) from the peak potential (E_{pa}) of DPV response.

2.1. *Synthesis of copper(II) complexes*

$[Cu(bba)(bpy)](ClO_4)_2$ (**1**): The complex **1** was prepared by adding a solution of copper(II) perchlorate hexahydrate (0.370 g, 1 mmol) in methanol (10 mL) to a 15 mL methanolic solution of 2,2′-bipyridine (bpy; 0.156 g, 1 mmol) and N,N-bis(benzimidazol-2-ylmethyl)amine (bba; 0.277 g, 1 mmol) and then stirring the solution for 2 h. The blue precipitate obtained was collected by suction filtration, washed with small amounts of cold methanol and diethyl ether and then dried in vacuum over P_4O_{10}. Yield: 0.45 g (65%). Λ_M (Ω^{-1} cm^2 mol^{-1}) in DMF at 25 °C: 160. μ_{eff} (solid, 298 K): 1.81 μ_B. ESI-MS (CH_3CN) displays a peak at m/z 248.35 $[Cu(bba)(bpy)]^{2+}$. Anal. Calc. for $C_{26}H_{23}N_7O_8Cl_2Cu$. C, 44.87; H, 3.33; N, 14.09. Found: C, 44.82; H, 3.37; N, 14.14%. FT-IR (KBr, cm^{-1}) selected bands: 1528 ν_{bzim}(C=N), 1638 ν_{bzim}(-C=N-C=C-), 1040, 1094 ν_{bzim}(C-N), 3245 ν_{amine}(N-H), 1556 ν_{py}(C=N), 1091, 625 $\nu(ClO_4^-)$. Electronic spectrum in 2% DMF - 5 mM Tris-HCl/50 mM NaCl buffer solution, λ_{max}/nm (ε_{max}/M^{-1} cm^{-1}): 271 (22680), 278 (24600), 311 sh, 635 (90). Molecular orbital coefficients such as α^2 (0.83), β^2 (0.70) and γ^2 (0.58) and orbital reduction factors viz. $K_{\|}$ (0.76) and $K_{\perp}$ (0.69).

The blue-colored crystals of **1** suitable for X-ray diffraction studies were obtained by dissolving the complex in DMF:MeCN mixture (1:5 v/v) and allowing it to crystallize at 5 °C for 12 days.

$[Cu(bba)(phen)](ClO_4)_2$ (**2**): The complex **2** was prepared by adopting the procedure used for obtaining **1** by using 1,10-phenanthroline (phen; 0.180 g, 1 mmol) instead of bpy. Yield: 0.43 g (60%). Λ_M (Ω^{-1} cm^2 mol^{-1}) in DMF at 25 °C: 161. μ_{eff} (solid, 298 K): 1.79 μ_B. ESI-MS (CH_3CN) displays a peak at m/z 260.43 $[Cu(bba)(phen)]^{2+}$. Anal. Calc. for $C_{28}H_{23}N_7O_8Cl_2Cu$. C, 46.71; H, 3.22; N, 13.62. Found: C, 46.79; H, 3.24; N, 13.69%. FT-IR (KBr, cm^{-1}) selected bands: 1546 ν_{bzim}(C=N), 1623 ν_{bzim}(-C=N-C=C-), 1044, 1081 ν_{bzim}(C-N), 3241 ν_{amine}(N-H), 1543 ν_{py}(C=N), 1084, 623 $\nu(ClO_4^-)$. Electronic spectrum in 2% DMF - 5 mM Tris-HCl/50 mM NaCl buffer solution, λ_{max}/nm (ε_{max}/M^{-1} cm^{-1}): 271 (33440), 278 (35900), 311 sh, 638 (130). Molecular orbital coefficients such as α^2 (0.82), β^2 (0.72) and γ^2 (0.60) and orbital reduction factors viz. $K_{\parallel}$ (0.77) and $K_{\perp}$ (0.70).

$[Cu(bba)(dpa)](ClO_4)_2$ (**3**): The complex **3** was prepared by adopting the procedure used for obtaining **1** by using 2,2'-dipyridylamine (dpa; 0.171 g, 1 mmol) instead of bpy. Yield: 0.47 g (66%). Λ_M (Ω^{-1} cm^2 mol^{-1}) in DMF at 25 °C: 165. μ_{eff} (solid, 298 K): 1.83 μ_B. ESI-MS (CH_3CN) displays a peak at m/z 255.92 $[Cu(bba)(dpa)]^{2+}$. Anal. Calc. for $C_{26}H_{24}N_8O_8Cl_2Cu$. C, 43.92; H, 3.40; N, 15.76. Found: C, 43.98; H, 3.49; N, 15.88%. FT-IR (KBr, cm^{-1}) selected bands: 1534 ν_{bzim}(C=N), 1632 ν_{bzim}(-C=N-C=C-), 1042, 1090 ν_{bzim}(C-N), 3218 ν_{amine}(N-H), 1549 ν_{py}(C=N), 1105, 621 $\nu(ClO_4^-)$. Electronic spectrum in 2% DMF - 5 mM Tris-HCl/50 mM NaCl buffer solution, λ_{max}/nm (ε_{max}/M^{-1} cm^{-1}): 254 (26930), 271 (25480), 312 (15050), 658 (125). Molecular orbital coefficients such as α^2 (0.81), β^2 (0.67) and γ^2 (0.52) and orbital reduction factors viz. $K_{\parallel}$ (0.73) and $K_{\perp}$ (0.65).

2.2. *X-ray crystallography*

The crystal of **1** with dimensions 0.42×0.28×0.12 mm^3 was selected under the polarizing microscope and then mounted on the tip of glass fiber and cemented using epoxy resin. Intensity data for **1** was collected using Mo-K_α (λ = 0.71073 Å) radiation on a Bruker SMART Apex diffractometer equipped with a CCD area detector at 296 K. The SMART program [28] was used for collecting frames of data, indexing the reflections, and determining the lattice parameters. The data integration and reduction were processed with SAINT [29] software. Empirical absorption correction was applied to the collected reflections with SADABS [30]. The structure was solved by direct methods using SHELXS-97 [31-33] and was refined on F^2 by the full-matrix least-squares technique using the SHELXL-97 [31-33] program package. All the non-hydrogen atoms in **1** were refined anisotropically until convergence is reached. Hydrogen atoms attached to the ligand moieties were stereochemically fixed. The crystallographic data and details of data collection for **1** are given in Table 1.

Table 1. Crystal data and structure refinement details for $[Cu(bba)(bpy)](ClO_4)_2$ (**1**).

empirical formula	$C_{26}H_{23}Cl_2CuN_7O_8$	Formula weight	695.95
crystal system	triclinic	space group	P-1
a, Å	9.120(3)	b, Å	10.506(4)
c, Å	16.767(6)	α, deg	83.346(6)
β, deg	74.488(6)	γ, deg	64.483(5)
V, Å	1396.9(9)	Z	2
λ, Å (Mo Kα)	0.71073	D_{calc}, g cm^{-3}	1.655
goodness-of-fit on F^2	1.054	θ for data collection (deg)	1.26-25.00
final R indices [I > 2σ(I)]	$R_1 = 0.0696$, $wR_2 = 0.1656$	R_1[a]	0.0871
wR_2[a]	0.1776		

[a] $R_1 = \Sigma ||F_o| - |F_c||/\Sigma|F_o|$, $wR_2 = \{\Sigma w[(F_o^2 - F_c^2)^2/\Sigma w[(F_o^2)^2]\}^{1/2}$.

2.3. *DNA binding experiments*

Solutions of DNA in the 2% DMF - 5 mM TrisHCl/50 mM NaCl buffer gave a ratio of UV absorbances at 260 and 280 nm, A_{260}/A_{280}, of 1.9, representing that the DNA was free from protein [34]. Concentrated stock solutions of DNA (13.5 mol dm^3) were prepared in the buffer and sonicated for 25 cycles, where each cycle consisted of 30 s with 1 min intervals. After 1:100 dilutions, the UV absorbance at 260 nm (ε_{260}, 6600 dm^3 mol^{-1} cm^{-1}) was used to estimate the concentration of DNA in nucleotide phosphate (NP). Stock solutions of DNA were kept at 4 °C and used within 4 days. Concentrated stock solutions of copper(II) complexes were prepared by dissolving calculated amounts of the complexes in respective amounts of DMF and diluted suitably with the corresponding buffer to the required concentrations for all experiments. For absorption and emission spectral experiments, the DNA solutions were pretreated with solutions of copper(II) complex to ensure no change in concentrations of the copper(II) complex.

Absorption spectral titration experiments were performed by maintaining a constant concentration of the complex and varying the nucleic acid concentration. This was achieved by dissolving an appropriate amount of the metal complex and DNA stock solutions while maintaining the total volume constant (1 mL). This results in a series of solutions with varying concentrations of DNA but with a constant concentration of the complex. The absorbance (A) of the UV band of the complex was recorded after successive additions of CT DNA.

Emission intensity measurements were carried out using a Shimadzu RF-5301PC spectrofluorophotometer. The 2% DMF - 5 mM Tris-HCl/50 mM NaCl buffer was used as a blank to make preliminary adjustments. Before measurements, the excitation wavelength was fixed and the emission range was adjusted. DNA was pretreated with ethidium bromide in the ratio [NP] : [EthBr] = 1:1 for 30 min at 27 °C. The metal complex was then added to this mixture and their effect on the emission intensity was measured.

2.4. *Protein binding experiments*

The UV-Visible absorption spectra of 1.0 μM free BSA as well as BSA/copper(II) complex (equal molar ratio) in 0.5 M phosphate buffer of pH 7.4 were recorded from 200-500 nm.

Quantitative analyses of the interaction between copper(II) complex and BSA was performed by fluorimetric titration (0.5 M phosphate buffer, pH 7.4). A 3.0 mL portion of the aqueous solution of BSA (1.0×10^{-6}mol L^{-1}) was titrated by successive additions of complex (to give a final concentration of 8.0×10^{-6}mol L^{-1}). Titrations were done manually by using an Eppendorf micropipette. For every addition, the mixture solution was shaken and allowed to stand for 20 min at the corresponding temperature (300 and 310 K), and then the fluorescence intensities were measured with an excitation wavelength of 280 nm and emission wavelengths in the interval 290-500 nm. No correction for inner filter effect was applied since copper(II) complex represented very low absorbance (less than 0.1) at excitation and emission wavelengths. The excitation and emission slit width (each 5.0 nm), scan rate (fast) were constantly maintained for all the experiments. In the meantime, the synchronous fluorescence intensity of the mixture solution was measured at $\Delta\lambda$ = 15 nm and $\Delta\lambda$ = 60 nm, respectively.

2.5. *DNA cleavage experiments*

The interaction of complexes with supercoiled pUC19 DNA was monitored using agarose gel electrophoresis. In reactions using supercoiled pUC19 DNA, the plasmid DNA (SC form, 20 μM) in 2% DMF - 5 mMTris-HCl/50 mMNaCl buffer solution at pH 7.2 was treated with copper complexes in the same buffer. In each experiment supercoiled pUC19 DNA was treated with different concentrations of complexes and also the cleavage of plasmid DNA in the absence and presence of the activating agent H_2O_2 was monitored using agarose gel electrophoresis. The samples were then incubated for 2 h at 37 °C and analyzed for the cleaved products using gel electrophoresis as discussed below. A loading buffer containing 22% bromophenol blue, 0.22% xylene cyanol and 30% glycerol (3 μL) was added and electrophoresis was performed at 40 V for 6 h in Tris-acetate-EDTA (TAE) buffer (40 mM Tris base, 20 mM acetic acid, 1 mM EDTA) using 1% agarose gel containing 1.0 μg mL^{-1} EthBr. The gels were viewed in a Gel doc system and photographed using a CCD camera (Alpha Innotech Corporation). The cleavage efficiency was measured by determining the ability of complexes to convert the supercoiled DNA (SC) to nicked circular form (NC) and linear form (LC). In order to identify the reactive oxygen species (ROS) involved in the cleavage reaction the radical scavengers such as hydroxyl radical (DMSO, 6 μL), singlet oxygen (NaN_3, 100 μM), superoxide (SOD, 4 unit), and H_2O_2 (catalase, 6 units) were introduced.

2.6. *Cell line*

The human cervical cancer cell line (HeLa) was acquired from National Centre for Cell Science (NCCS), Pune. It was grown in Eagles Minimum Essential Medium containing 10% fetal bovine serum (FBS). The cells were preserved at 37 °C, 5% CO_2, 95% air and 100% relative humidity. Maintenance cultures were channelized weekly and the culture medium was altered twice a week.

2.7. *Cell culture*

To make single cell suspensions, the monolayer cells were detached with trypsin-ethylenediaminetetraacetic acid (EDTA) and viable cells were counted using a hemocytometer. They were diluted with medium containing 5% FBS to give a final density of 1×10^5 cells/mL. The cell suspension of one hundred microlitres per well were seeded into 96-well plates at a plating density of 10,000 cells/well. They were incubated to allow for cell attachment at 37 °C, 5% CO_2, 95% air and 100% relative humidity. The cells were treated with serial concentrations of the test samples after 24 h. They were dissolved in dimethylsulfoxide (DMSO) and an aliquot of the sample solution was diluted twice to the desired final maximum test concentration with serum-free medium. Also, four serial dilutions were made to give a total of five sample concentrations. Aliquots of 100 µL of different sample dilutions were added to the suitable wells already containing 100 µL of the medium, resulting in the required final sample concentrations. The plates were incubated followed by sample addition at 37 °C, 5% CO_2, 95% air and 100% relative humidity for an additional 48 h. The medium alone was served as control and triplicate was maintained for all concentrations.

2.8. *Cell viability assay*

The cell viability was carried out by using the MTT assay. Complex **1-3** in the concentration range 0.25-100 µM dissolved in 2% DMF: 5 mMTris-HCl/50 mMNaCl buffer at pH 7.1 were added to the wells 24 h after seeding of 1×10^5 cells per well in 100 µL of fresh culture medium. After 48 h, 15 µL of 3-[4,5-dimethylthiazol-2-yl]2,5-diphenyltetrazolium bromide (MTT, 5 mg/mL) in phosphate buffered saline (PBS) was added to each well and incubated at 37 °C for 4 h. The formed formazan crystals were solubilized in 100 µL of DMSO after the medium with MTT was flicked off. The microplate reader was used to measure the absorbance at 570 nm. Data were collected for three replicates each and the percentage cell viability and percentage cell inhibition was calculated using the following formulas:

% Cell viability = $[A_s] / [A_c] \times 100$ (where A_s is absorbance of sample and A_c is absorbance of control).

% Cell inhibition = $[100 - ([A_s] / [A_c])] \times 100$

Nonlinear regression graph was plotted between % Cell inhibition and Log concentration and IC_{50} was calculated using GraphPad Prism software.

3. Results and Discussion

3.1. *Synthesis and general properties*

The mixed ligand copper(II) complexes have been isolated in good yield (60-66%) by the reaction of bba and bpy or phen or dpa and copper(II) perchlorate hexahydrate in methanol at room temperature. All the complexes have been obtained as blue crystalline solids. Based on the elemental analysis the complexes were formulated as $[(Cu(bba)(diimine)](ClO_4)_2$ and the stoichiometry of **1** was confirmed by single crystal X-ray structure determination. They show strong infrared spectral bands in the range 1528-1546 cm^{-1} and 1623-1638 cm^{-1} are assigned to ν_{bzim}(C=N) and ν_{bzim}(-C=N-C=C-) stretching vibrations respectively of the benzimidazole ring. The very strong band (1040-1048 cm^{-1}) and a medium band (1081-1094 cm^{-1}) are assigned to ν_{bzim}(C-N) stretching vibrations. The band in the range 3218-3245 cm^{-1} is due to ν_{amine}(N-H) stretching mode of bba ligand while the sharp and strong band (1543-1556 cm^{-1}) is assigned to ν_{py}(C=N) stretching vibration of diimine ligands. The shift in the vibrational bands to lower energy implies the coordination of amine, benzimidazole, and pyridine nitrogens. A broad intense band (1084-1105 cm^{-1}) and a strong sharp band (623-625 cm^{-1}) are observed, which are characteristics of non-coordinated perchlorate ions. The μ_{eff} values (1.79-1.83 μB) are typical of paramagnetic, mononuclear copper(II) species with d^9 configuration [35]. The ESI-MS data in MeCN (m/z $[Cu(bba)(diimine)]^{2+}$: **1**, 248.35; **2**, 260.43; **3**, 255.92) reveal that the complexes maintain their identity in solution and this is substantiated by values of molar conductivity in DMF (Λ_M/Ω^{-1} cm^2 mol^{-1}: 160-165), characteristics of 1:2 electrolytes [36].

3.2. *Description of the crystal structure*

The ORTEP view (Fig. 1a) of **1** shows a discrete monomeric copper(II) complex dication and two perchlorate anions. The selected bond distances and bond angles relevant to the copper coordination sphere are given in Table 2.

Table 2.Selected interatomic distances [Å] and bond angles [°] for $[Cu(bba)(bpy)](ClO_4)_2$ (**1**).

Cu(1)-N(1)	1.997(4)	Cu(1)-N(2)	1.994(4)	Cu(1)-N(3)	1.987(4)
Cu(1)-N(4)	1.985(4)	Cu(1)-N(7)	2.412(5)		
N(4)-Cu(1)-N(3)	87.03(17)	N(4)-Cu(1)-N(2)	170.66(16)	N(3)-Cu(1)-N(2)	96.22(17)
N(4)-Cu(1)-N(1)	95.15(17)	N(3)-Cu(1)-N(1)	176.82(16)	N(2)-Cu(1)-N(1)	81.28(17)
N(4)-Cu(1)-N(7)	77.50(17)	N(3)-Cu(1)-N(7)	78.90(18)	N(2)-Cu(1)-N(7)	111.69(17)
N(1)-Cu(1)-N(7)	103.82(17)				

The value of the structural index [37] τ of 0.10 reveals that the coordination geometry around copper(II) is best described as square pyramidal [38,39] with no significant distortion toward trigonalbipyramidal. The tridentate ligand bba is bound facially to Cu(II) with the two bzim nitrogens (Cu-N_{bzim}, 1.987(4), 1.985(4) Å) located in the basal plane and the two imine nitrogens of bpy (Cu-N_{imine}, 1.997(4), 1.994(4) Å) occupying the remaining corners of the basal plane. The strongly bound bpynitrogens occupy the equatorial sites around Cu(II) with the sterically hindered N7 amine nitrogen atom of bba defaulting to the more weakly bound z-axial position (Cu(1)-N(7), 2.412(5) Å) [27]. The displacement of copper atom above the N1N2N3N4 plane is 0.094 Å illustrating the importance of the steric effect of the bulky bzim moieties. The Cu-N_{bzim} bond distances are similar to those observed for $[Cu(bba)Cl_2]$ [40,41] and $[Cu(bba)_2]^{2+}$ [27]. The axial Cu-N_{amine} bond is longer than the equatorial Cu-N_{bpy} bonds, which is expected of the presence of two electrons in the d_{z^2} orbital of Cu(II).

Interestingly, the molecular packing of **1** show two different self-assembled molecular associations between different adjacent molecules, viz. interactions between the molecules I and II and II and III (Fig. 1b).

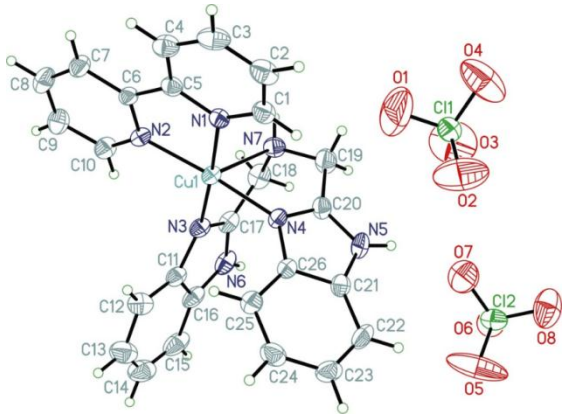

(a)

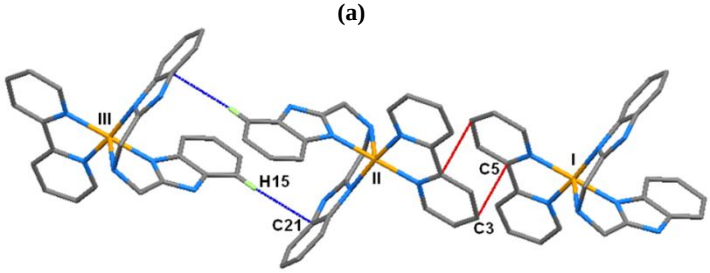

(b)

Fig. 1. (a) An ORTEP view of $[Cu(bba)(bpy)](ClO_4)_2$ **1** with atom numbering of complex and thermal ellipsoids at 40% probability. (b) Molecular packing viewed down the a-axis showing intermolecular interactions of $[Cu(bba)(bpy)]^{2+}$ (**1**) (**Blue**, C-H···π; **Red**, π···π stacking).

The noticeable features are the presence of (i) inter-pair π-π interactions between bpy ligands (I and II) and (ii) C-H···π non-covalent interactions (II and III). The π-π stacking between C(3) of py and C(5) of py (C(3)···C(5), 3.393 Å) rings of adjacent coordinated bpy ligands giving an average spacing of $C_g(p)\cdots C_g(p)$ ($C_g(p)$, the centroid of the pyridine ring; 3.546 Å). Such an interaction is expected to stabilize the complex in the solid state [42]. Also, benzene rings of benzimidazole moiety of neighboring molecules display an attractive C-H···π non-covalent interaction. It gives C(15)-H(15)···C(21) distance of 3.654 Å and the C(15)-H(15)···C_g(benzene) distance of 3.856 Å and ∠C(15)-H(15)···C_g(benzene) angle of 160.02° (C_g(benzene) is the centroid of the benzene in benzimidazole moiety) showing the closure approach and orientation of the neighbouring molecules [43]. Thus, the separation of Cu···Cu between the adjacent molecules is 8.15 (I and II) and 10.69 Å (II and III).

3.3. *Electronic and EPR spectral properties*

The complexes (**1**-**3**) exhibit only one broad band (λ_{max}, 639-667 nm) in the visible region with very low ε_{max} value (70-120 M^{-1} cm^{-1}), which is typical of a distorted square-based coordination geometry around copper(II). The strong absorption band is observed in the UV region (λ_{max}, 269-315 nm), which is attributing to the intraligand$\pi\rightarrow\pi^*$ transitions [44] from the coordinated diimines. The EPR spectra of **1**-**3** display one broad singlet (g_{iso}, 2.053-2.066) in the polycrystalline state at 298 K arising from dipolar broadening and enhanced spin-lattice relaxation. The frozen DMF solution EPR spectra of the complexes are axial [$g_{\|}>g_{\perp}>$ 2.0; G = [($g_{\|}$ - 2)/($g_{\perp}$- 2)] = 4.9-5.1] suggesting the presence of $d_{x^2-y^2}$ ground state in copper(II) located in square-based geometries [45]. A square-based CuN_4 chromophore is expected [46-48] to show a $g_{\|}$ value of 2.200 and $A_{\|}$ value in the range 180-200 × 10^{-4} cm^{-1} and a tetrahedral distortion from square planar coordination geometry or axial interaction would increase both the ligand field band position (cf. above) and $g_{\|}$ value and decrease the $A_{\|}$ value [46-48]. So, the observed values of $g_{\|}$ (~2.25) and $A_{\|}$ (181-186 × 10^{-4} cm^{-1}) for **1**-**3** are consistent with the presence of a square-based CuN_4 chromophore with no significant distortion from planarity, as evident from the crystal structure of **1** (cf. above). This is supported by the values of $g_{\|}/A_{\|}$ quotient (122−124 cm) falls in the range of 105–135 cm [49]. Molecular orbital coefficients [50], α^2 (covalent in-plane σ-bonding: **1**, 0.83; **2**, 0.82; **3**, 0.81) and β^2 (covalent in-plane π-bonding; **1**, 0.70; **2**, 0.72; **3**, 0.67) values show that there is a considerable interaction in the in-plane σ-bonding while the in-plane π-bonding is nearly covalent. For complexes **1**-**3**, it is observed that $K_{\|}>K_{\perp}$ [51] ($K_{\|}$ (**1**, 0.76; **2**, 0.77; **3**, 0.73) and $K_{\perp}$ (**1**, 0.69; **2**, 0.70; **3**, 0.65) are orbital reduction factors), illustrating the significant out-of-plane π-bonding.

3.4. *Electrochemical properties*

The complexes are redox-active and show a one-electron quasi-reversible (ΔE_p: **1**, 198; **2**, 128; **3**, 206 mV) cyclic voltammetric responses in DMF for the Cu(II)/Cu(I) couple ($E_{1/2}$: **1**, -0.074; **2**, -0.074; **3**, -0.072 V vs SCE) with an i_{pa}/i_{pc} ratio (**1**, 0.9; **2**, 1.0; **3**, 0.9) of

unity. Though the $E_{1/2}$ values are similar, the E_{pa} (**1**, -0.173; **2**, -0.138; **3**, -0.175 V) and E_{pc} (**1**, 0.025; **2**, -0.010; **3**, 0.031 V) values suggest the stability order for the copper(I) species as **2** (phen) >**1** (bpy) >**3** (dpa). A greater stabilization of the Cu(I) species for the phen complex is related to the planar phenyl moiety enhancing the π-acidity of the ligand. Notably, **2** shows very low ΔE_p value compared to **1** and **3**, demonstrating the minimal structural reorganization between copper(II) and copper(I) species. It leads to a facile heterogeneous electron transfer [52] possibly due to the equatorial coordination of planar phen and bulky benzimidazoles of bba.

3.5. *DNA binding studies*

DNA is an important cellular target of many metallodrugs for the treatment of multiple pathologies including cancer. Thus, the binding ability of the complexes **1**-**3** with calf thymus (CT) DNA is characterized by measuring the effects on absorption, emission, and circular dichroism spectral and electrochemical techniques. The absorption spectra of **1**-**3** in the absence and presence of CT DNA at different concentrations R=25 (R=[DNA] / [Cu complex]; Fig. 2) show interesting changes in the intensity of intraligand absorption band (268 nm). This suggests the hypochromism for **1**-**3**, typical of metal complex's association with the DNA helix. The strong hypochromic effect (61%) along with the 3 nm red shift for **2** reveals the partial intercalative [53] interaction through the active participation of planar phen moiety with DNA. However, the lack of red shift suggests that the binding mode of **1** and **3** (hypochromic effect: **1**, 56; **3**, 48%) was not intercalative. Because of the bulky structure of the complexes as well as the co-lignad is non-planar bpy (**1**) or dpa (**3**), the bzim rings cannot completely intercalate. When one of the two bzim rings inserts into the helix, the other ring extends away from the plane due to the stereochemistry effect and hence decreasing the effective area of overlap. Therefore, the observed spectral changes were rationalized in terms of feeble intercalation via bzim moiety in **1** and **3**. To further illustrate the DNA binding strength, the intrinsic binding constant K_b was determined for **1**-**3** which were found to be 3.26×10^4 M^{-1} (**1**), 3.49×10^4 M^{-1} (**2**), 3.11×10^4 M^{-1} (**3**). The binding constants were lower compared to classical intercalators (EthBr-DNA, 1.4×10^6 M^{-1}) [54], the diminution could be explained by the steric constraints imposed by the ligand framework and thus encouraging a partial intercalative binding mode for these complexes and it was found for many other compounds with the same order of K_b values [55].

The observed circular dichroic (CD) spectrum of CT DNA consists of a positive band at 273 nm owing to base stacking and a negative band at 243 nm owing to helicity which is typical of DNA in right-handed B-form. Upon incubation of CT DNA with **1**-**3**, shows conformational changes: (i) the intensity of both the bands of CT DNA increases (**1** and **3**) with the red shift of 2-3 nm in the positive band and (ii) the intensity of positive band increases while the intensity of the negative band decreases (**2**) with the red shift of 3 nm in the positive band (Fig. 3). These observations are consistent with the partial

intercalative interaction through planar phen moiety (**2**) or bzim moiety (**1** and **3**) supporting the results from UV-vis spectroscopy.

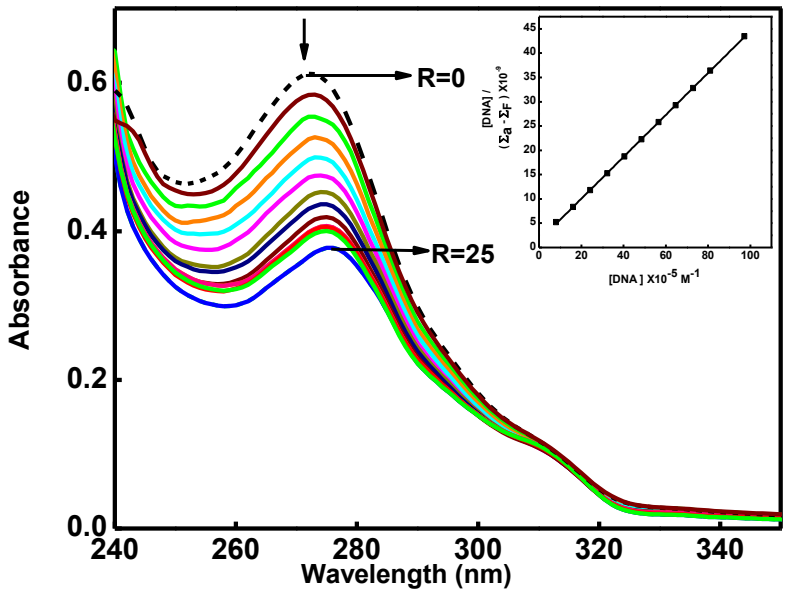

Fig. 2. Absorption spectra of **2** (2.7×10^{-5} M) in 2% DMF/5mM Tris-HCl/50 mMNaCl buffer at pH 7.1 in the absence (R = 0) and presence (R = 25) of increasing amounts of CT DNA. Inset: Plot of [DNA] vs [DNA]/(ε_a - ε_f) at R = 25 of **2.**

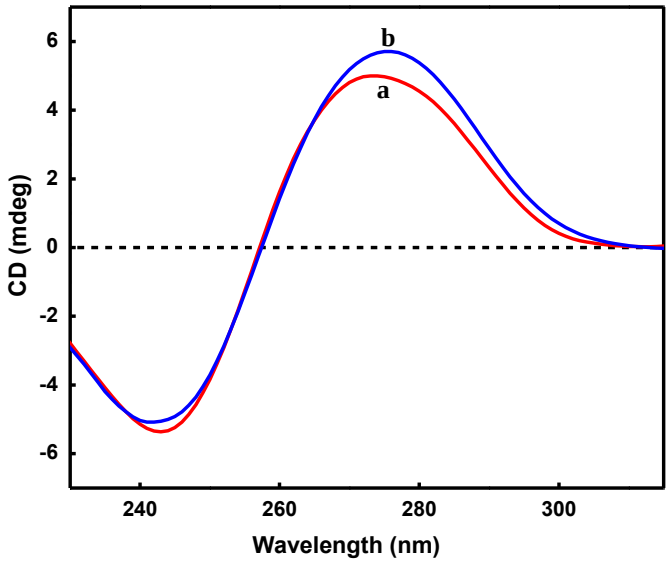

Fig. 3. Circular dichroism spectra of CT DNA in 2% DMF/5mM Tris-HCl/50 mMNaCl buffer at pH 7.1 and 25 °C in absence (a) and presence (b) of **2** at 1/R value of 3.

In competitive DNA binding experiment, with increasing amounts of **1**-**3**, the fluorescence intensity of CT DNA-EthBr system (594 nm) was quenched (**1**, 89; **2**, 96; **3**, 76%) with the red shift of 5 nm (**2**) or 1 nm (**1**) or no shift (**3**), which was due to the partial intercalation of copper(II) complexes to DNA base pairs displacing some EthBr from CT DNA-EthBr system (Fig. 4) [56]. The quenching data (K_{sv}) were analyzed according to the Stern-Volmer equation and the binding constant (K_{app}) value obtained using the equation, K_{EthBr}[EthBr] = K_{app}[Cu(II) Complex]. The K_{sv} (**1**, 1.55×10^4; **2**, 5.40×10^4; **3**, 1.01×10^4 M^{-1}) and K_{app} (**1**, 1.54×10^5; **2**, 2.06×10^5; **3**, 1.03×10^5 M^{-1}) values indicate that the complex **2** binds more strongly (*via* planar phen moiety) than the complexes **1** and **3** (*via* bzim moiety) through partial intercalative mode.

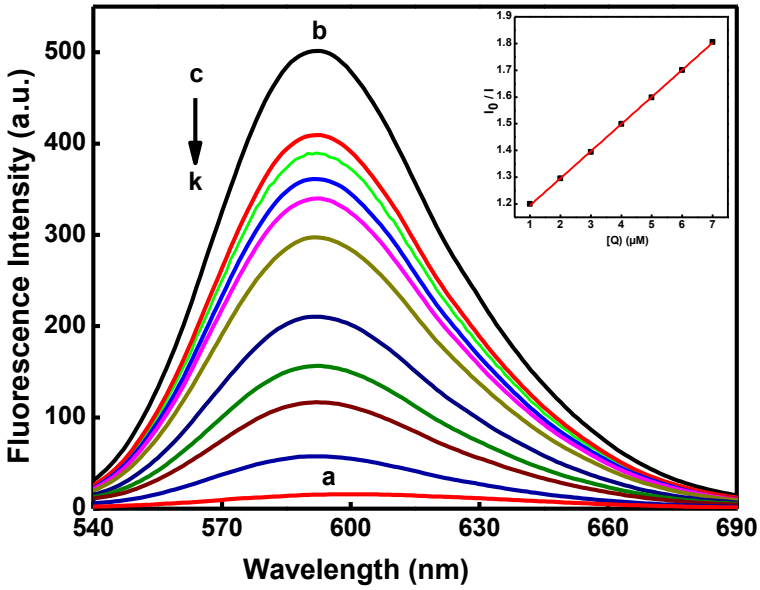

Fig. 4. Fluorescence quenching curves of ethidium bromide bound to DNA in 2% DMF/5mM Tris-HCl/50 mMNaCl buffer at pH 7.1: (a) EthBr (1.25 μM); (b) EthBr+DNA (125 μM); (c-k) EthBr+DNA+ **2** (0-10 μM). Inset: Plot of I_O/I vs [complex] of **2**.

The cyclic voltammograms of the complexes in the absence of DNA reveal a non-Nernstian but a fairly quasi-reversible (ΔE_p: **1**, 110; **2**, 128; **3**, 111 mV) one electron redox process (i_{pa}/i_{pc}: **1**, 1.0; **2**, 1.2; **3**, 1.0) involving the Cu(II)/Cu(I) couple ($E_{1/2}$: **1**, -0.089; **2**, -0.091; **3**, -0.085 V vs SCE). Upon the addition of excess DNA (R = 5), the complexes show a significant reduction in both cathodic and anodic peak currents and reveal quasi-reversible (ΔE_p: **1**, 156; **2**, 129; **3**, 116 mV) one electron (i_{pa}/i_{pc}: **1**, 1.0; **2**, 1.1; **3**, 1.2) electrochemical behavior for Cu(II)/Cu(I) couple ($E_{1/2}$: **1**, -0.193; **2**, -0.191; **3**, -0.198 V vs SCE). Interestingly, the reduction in both the peak currents indicates that the complexes bind through the partial intercalative mode and causes slow diffusion of an equilibrium mixture of the free and DNA-bound complexes to the electrode surface.

Further, the observed shifts (104-127 mV) in $E_{1/2}$ values (DPV) to more negative potentials (Fig. 5) suggest that both Cu(II) and Cu(I) forms of the present complexes bind to DNA but with Cu(II) displaying higher DNA binding affinity than Cu(I) form, which is substantiated by the ratio of the equilibrium constants (K_+/K_{2+}) [57]. The K_+/K_{2+} values (**1**, 0.02; **2**, 0.02; **3**, 0.01) are far less than unity suggesting preferential stabilization of Cu(II) form over Cu(I) form on binding to DNA.

3.6. *Protein binding studies*

Three intrinsic flours present in the protein, such as tryptophan, tyrosine and phenylalanine residues are responsible for the fluorescence of protein. Actually, the intrinsic fluorescence of many proteins is caused mainly by tryptophan alone. Fluorescence quenching corresponds to any process, which is a reduction of the fluorescence intensity from a fluorophore due to a variety of molecular interactions such as molecular rearrangements, reactions at excited-state, energy transfer ground-state complex formation and collisional quenching. Thus, the emission spectra of BSA (λ_{em}, 340 nm; λ_{ex}, 280 nm) in the presence of increasing concentrations of **1**-**3** were recorded at 300 K and 310 K.

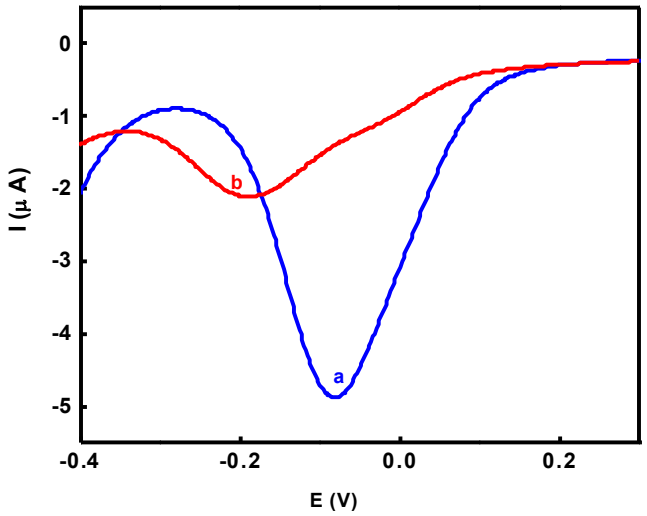

Fig. 5. Differential pulse voltammograms of **2** (0.5 mM) in the absence (a) and presence (b) of CT DNA (R = 5) at 25.0 ± 0.2 °C at 2 mV s^{-1} scan rate in 2% DMF/5mM Tris-HCl/50 mMNaCl buffer at pH 7.1.

The fluorescence intensity of BSA decreased regularly (Fig. 6), up to 61.6-74.4% (300 K) and 67.2-71.0% (310 K), accompanied by a hypsochromic shift of 3-14 nm (**1** and **2**) and bathochromic shift of 4-9 nm (**3**). The Stern-Volmer plots are linear [K_{SV}: 300 K, 3.16 (**1**); 2.45 (**2**); 2.01 × 10^5 M^{-1} (**3**) and 310 K, 3.58 (**1**); 2.79 (**2**); 2.15 × 10^5 M^{-1} (**3**)] and suggest that a single quenching mechanism, either static or dynamic is occurred at these concentrations [58]. The quenching rate constant (k_q) is on the order of 10^{13} $M^{-1}s^{-1}$, which

is 1000-fold higher than the maximum limit (2.0×10^{10} $M^{-1}s^{-1}$) [59], which indicates that the quenching is not initiated by dynamic collision but from the formation of the complex. On the other hand, upon addition of **1**-**3** to BSA, a significant decrease in 210 nm absorbance peak of BSA is observed (Fig. 7), which is attributed, to the induced perturbation of α-helix of BSA.

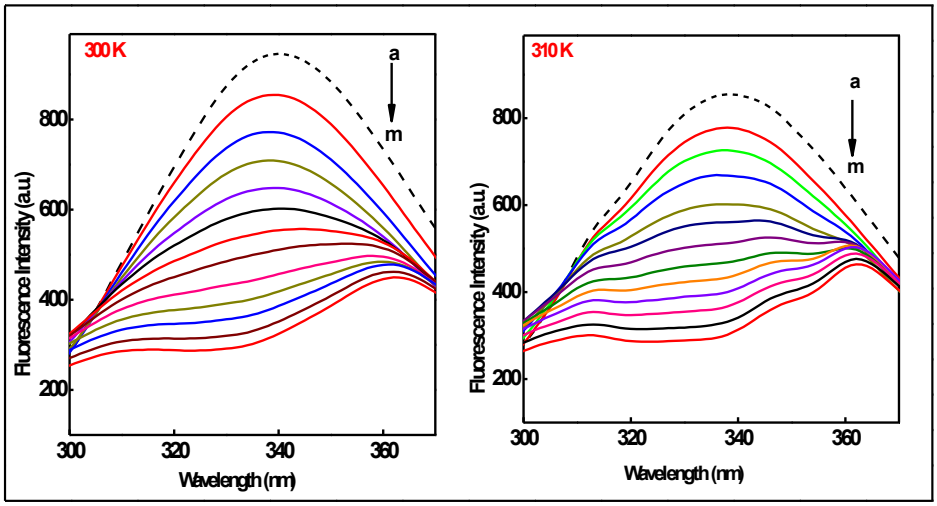

Fig. 6. Changes in the fluorescence spectra of BSA through the titration with **2** at 300 K (left), and 310 K (right). The concentration of BSA is 1×10^{-6} mol L^{-1}, and the concentration of **2** was varied from (a) 0.0 to (k) 4.0×10^{-6} mol L^{-1}; pH 7.4 and λ_{ex} 280 nm.

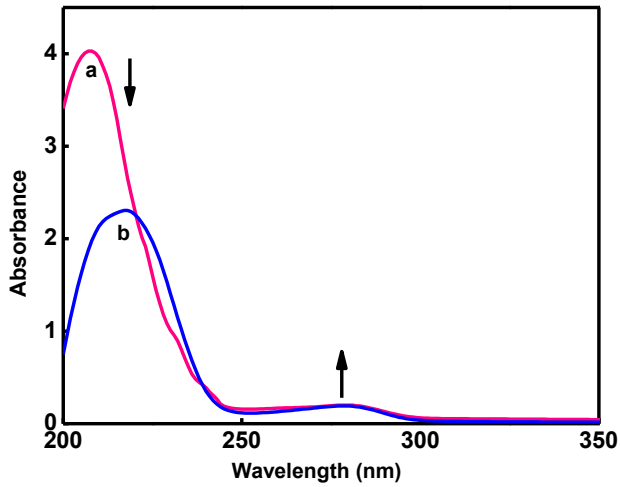

Fig. 7. UV-Vis absorption spectra of BSA in the absence and presence of **2**. (a) Absorption spectrum of BSA. (b) Absorption spectrum of BSA in the presence of **2** at the concentration, [BSA] = [Cu complex] = 3.5×10^{-6} mol L^{-1}.

Meanwhile, the absorption intensity of the 280 nm band is increased due to the alteration in the microenvironment of three amino acid residues followed by the disturbance of the tertiary structure of BSA. Therefore the interaction between **1**-**3** and BSA leads to an adduct species which undergoes mainly a static quenching process [60]. The binding constant K_b is decreased with increasing temperature [300 K, 0.83 (**1**); 0.73 (**2**); 1.42×10^5 M^{-1} (**3**) and 310 K, 0.42 (**1**); 0.60 (**2**); 0.78×10^5 M^{-1} (**3**)], which indicates the formation of stable BSA-(**1**/**2**/**3**) adduct and the number of binding site n is equal to 0.9 corresponds to the existence of a single binding site. So, the results suggest that the complex binds to the hydrophobic pocket located in subdomain IIA [61]. In order to elucidate the interaction forces of **1**-**3** with BSA, the thermodynamic parameters were calculated. The spontaneity of the interaction is revealed by negative ΔG value. The positive values obtained for both ΔH and ΔS indicates that a hydrophobic association is the major binding force and that the interaction is entropy driven process [62]. Therefore, hydrophobic forces may play the main role in binding of **1**-**3** to BSA. In addition to hydrophobic interaction, a possible covalent bonding may be also considered, instead, the ΔH value obtained (78-79 kJ mol^{-1}) is less than the expected value for a covalent bond formation (≥120 kJ mol^{-1}) [63].

According to the theory of Miller [64], when Δλ between excitation wavelength and the emission wavelength is set at 15 or 60 nm, the synchronous fluorescence gives information about the molecular environment in a vicinity of tyrosine and tryptophan residues, respectively. The synchronous fluorescence spectra of BSA with various amounts of **1**-**3** were recorded at Δλ = 15 nm and Δλ = 60 nm (Fig. 8). It is apparent that the emission maxima of tyrosine and tryptophan residues have significant blue-shifted (tyrosine: **1**, 314-299; **2**, 314-308; **3**, 314-303 nm and tryptophan: **1**, 346-338; **2**, 346-343; **3**, 346-339 nm). The blue-shift expressed that the conformation of BSA was changed, leading to the decrease in polarity and increase in hydrophobicity around the tyrosine and tryptophan residues. For BSA-(**1**/**2**/**3**) system, the synchronous fluorescence quenching ratios, RSFQ at Δλ = 60 nm (**1**, 74.7; **2**, 70.3; **3**, 72.1%) is greater than the corresponding one for Δλ = 15 nm (**1**, 55.0; **2**, 45.6; **3**, 60.1%), indicating that **1**-**3** reached sub-domain IIA, where the only one Trp 212 residues on BSA was located.

In order to estimate the distance between the buried Trp-212 (as donor) and the interacted complex (as acceptor), Förster's non-radiative energy transfer theory (FRET) [65] was adopted. The overlap of the UV absorption spectra of Cu(II) complexes with the fluorescence emission spectra of BSA is made. The energy transfer efficiency is not only depending on the distance between the donor and acceptor, but also to the critical energy transfer distance (r), which should be less than 8 nm. According to the Förster's equations, we obtain J(λ) (**1**, 4.33; **2**, 8.02; **3**, 3.08×10^{15} $M^{-1}cm^3$), R_0 (**1**, 1.46; **2**, 3.18; **3**, 2.06 nm), E (**1**, 0.18; **2**, 0.09; **3**, 0.08) and r (**1**, 6.61; **2**, 3.80; **3**, 2.14 nm). The donor (Trp 212 in BSA) to acceptor (**1**-**3**) distance (r) is less than 8 nm [60], indicates that the non-radiative energy transfer from BSA to Cu(II) complexes occurs with high possibility. These accord with the conditions of FRET, indicating again the static quenching interaction between Cu(II) complexes and BSA [66].

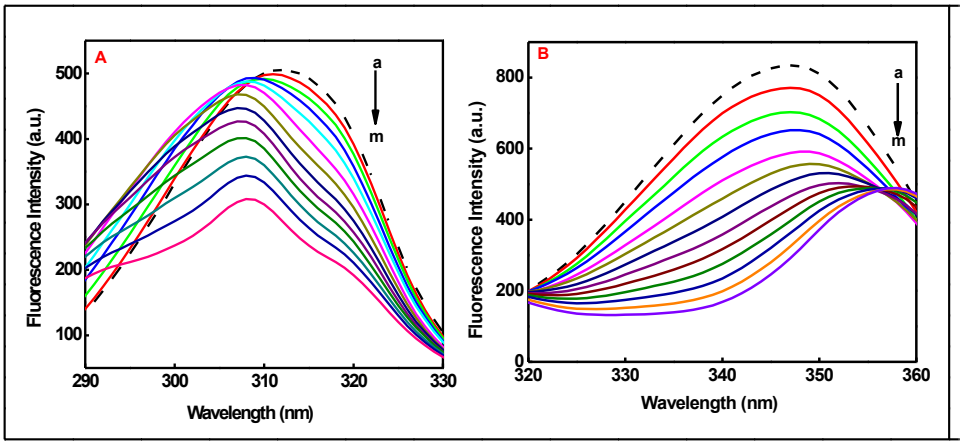

Fig. 8.Synchronous fluorescence spectra of BSA (1×10^{-6} mol L^{-1}) upon addition of **2**; $\Delta\lambda$ = 15 nm (left, **A**) and $\Delta\lambda$ = 60 nm (right, **B**). The concentration of **2** varied from (a) 0.0 to (j) 4.0×10^{-6} mol L^{-1}.

3.7. *DNA cleavage studies*

The complex concentrations in the range 5-500 μM, **1**-**3** fail to show any cleavage (Fig. 9) when supercoiled (SC) pUC19 DNA (20 μM) was incubated with them in the absence of an activator in 2% DMF/5 mMTris-HCl/50 mMNaCl buffer at pH 7.1 for 1 h at 37 °C. Therefore, the ability of **1**-**3** to cause DNA cleavage was studied in the presence of H_2O_2. In control experiments with DNA alone or DNA with H_2O_2 alone no DNA cleavage is observed. At lower complex concentrations, **1** (20 μM), **2** (12 μM) and **3** (30 μM) convert SC DNA into nicked circular (NC) form and then to linear open circular (LC) form (Fig. 10) revealing the efficient cleavage like activity. As concentrations of **1**-**3** are increased, the amount of form I decrease while both forms II and III increase. Interestingly, even at 12 μM concentration, the cleavage ability of **2** is found to be more efficient and also exhibits the same percentage of cleavage of DNA from the form I to form II as in **1** and **3**. The difference in the cleavage activity is due to the binding efficiency of the complexes to DNA (cf. Above). It means that **2** can intercalate into DNA owing to favorable planarity of the ligand phen, and that copper cation may coordinate with the negatively charged oxygen in the phosphodiester backbone of DNA, displacing a water molecule, which enhances the binding affinity between **2** and DNA. In the presence of H_2O_2 as a reducing agent, Cu(II) complex is first reduced to form Cu(I) species and bound to DNA [67], which reacts readily with H_2O_2 to produce a peroxide complex such as DNA-Cu(I)OOH [68]. In the proximity of DNA, furthermore, the reduction of the peroxide complex (DNA-Cu(I)OOH) produces the ROS in abundance, i.e., hydroxyl radical, •OH, which would immediately attack the adjacent deoxyribose ring in the DNA skeleton. The preliminary mechanism of DNA strand scission by **1**-**3** has been investigated in the presence of several additives such as DMSO, superoxide dismutase (SOD), NaN_3, and catalase. It is

remarkable that SOD, NaN_3 and catalase are ineffective, rule out the possibility of DNA cleavage by $^1O_2$ or O_2^- or H_2O_2 and imply that •OH radicals are playing a role in the DNA cleavage reaction (Fig. 11). The strongly DNA bound complex **2** (through partial intercalation *via* planar phen moiety) is located near the cleavage site is stabilized more in the Cu(I) state and so shows higher DNA cleavage compared to **1** and **3** (through partial intercalation *via* bzim moiety) using the availability of H_2O_2 since H_2O_2 is needed for both oxidation and reduction steps.

3.8. *In Vitro cytotoxicity studies*

Several copper(II) complexes display efficient cytotoxic action and anticancer properties due to the higher DNA binding affinity and prominent DNA cleavage activity [69,70]. Thus, as all the complexes strongly bind to DNA and induce efficient DNA cleavage, their cytotoxicity against human cervical carcinoma (HeLa) cell line has been investigated in comparison with the widely used drug cisplatin under identical conditions by using MTT assay. Their cytotoxicity was found to be concentration-dependent (0.25 to 100 μM) for 48 h incubation, which results in an increase in the percentage of cell inhibition (Fig. 12 CC).

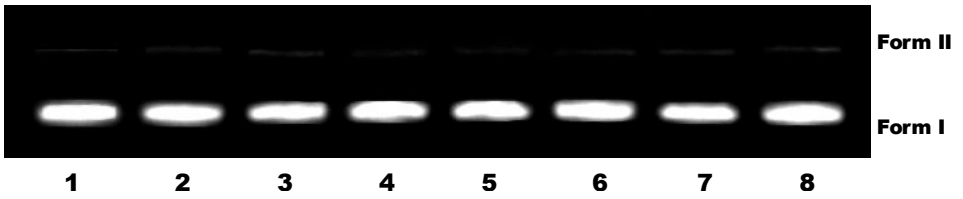

Fig. 9. Agarose gel showing cleavage of 20 μM SC pUC19 DNA incubated with **2** in 2% DMF/5 mMTris-HCl/50 mMNaCl buffer at pH 7.1 and 37 °C for 1 h. Lane 1, DNA control; lanes 2-8, DNA+**2** (5, 10, 50, 100, 200, 300, 500 μM respectively). Forms I and II are supercoiled and nicked circular forms of DNA respectively.

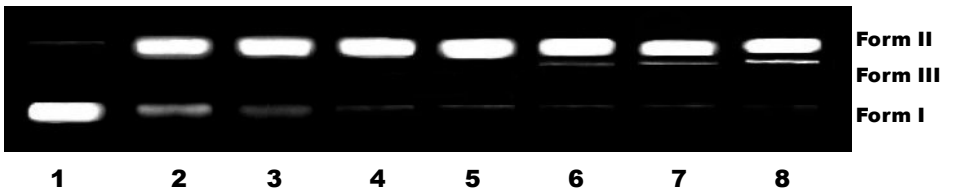

Fig. 10. Agarose gel showing cleavage of 20 μM SC pUC19 DNA incubated with **2** in 2% DMF/5 mMTris-HCl/50 mMNaCl buffer at pH 7.1 and 37 °C in the presence of H_2O_2 (200 μM). Lane 1, DNA+H_2O_2; lanes 2-8, DNA+H_2O_2+**2** (1, 2, 4, 6, 8, 10, 12 μM respectively). Forms I, II and III are supercoiled, nicked circular and linear forms of DNA respectively.

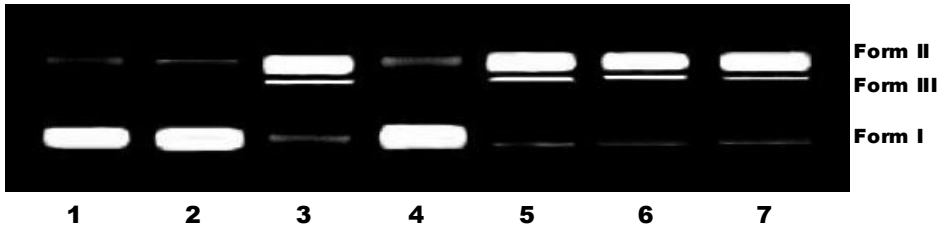

Fig. 11. Gel electrophoresis diagram showing the cleavage of 20 μM SC pUC19 DNA by **2** (12 μM) in a 2% DMF/5 mMTris-HCl/50 mMNaCl buffer at pH 7.1 and 37 °C in the presence of H_2O_2 (200 μM) with an incubation time of 2 h: lane 1, DNA control; lane 2, DNA+**2**; lane 3, DNA+**2**+H_2O_2; lane 4, DNA+**2**+H_2O_2+DMSO (20 μM); lane 5, DNA+**2**+H_2O_2+SOD (0.5 units); lane 6, DNA+**2**+H_2O_2+NaN_3 (100 μM); lane 7, DNA+**2**+H_2O_2+Catalase (6 unit).

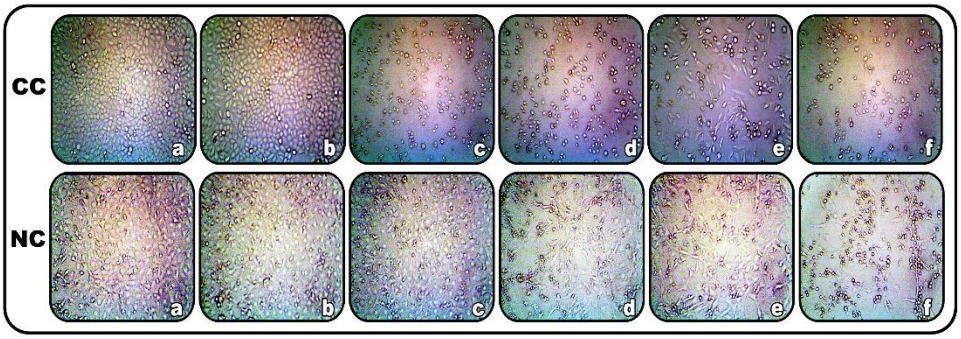

Fig. 12. Photomicrograph of human cervical carcinoma cell line (HeLa; **CC**) and normal mouse embryonic fibroblasts cell line (NIH 3T3; **NC**) after 48 h exposure with **2.**
CC (a, control; b, 0.25 μM; c, 2.5 μM; d, 25 μM; e, 50 μM; f, 100 μM).
NC (a, control; b, 0.1 μM; c, 1.0 μM; d, 10 μM; e, 50 μM; f, 100 μM).

The IC_{50} values obtained reveal that the potency of the complexes to kill the cancer cells follows the order **2**>**1**>>**3**, disclosing that the mode and extent of interaction of complexes with DNA dictate the cell killing ability (cf. above). The cell killing ability with **2** and **1** is remarkable in displaying cytotoxicity (IC_{50}: **2**, 2.17 (0.26); **1**, 8.33 (0.16) μM), approximately 8 and 2 times more potent respectively than cisplatin (IC_{50}, 16.41 (0.21) μM) [3] whereas **3** (IC_{50}, 20.82 (0.09) μM) show relatively lower cytotoxicity. Notably, the highly remarkable cytotoxicity of **2** compares to **1** and **3** is attributed to the stronger binding of the complex through the partial intercalative insertion of planar phen ring between the base pairs and its higher cleavage activity is responsible for its potency to induce cell death. As a measure of therapeutic potential, we further determined the cytotoxicity of **1**-**3** against normal mouse embryonic fibroblasts cell line NIH 3T3 (Fig. 12 NC). In general, they do not cause any damage toward NIH 3T3 (IC_{50}> 100 μM), indicating that they are non-toxic to healthy cells, which is expected for a better drug.

4. Conclusion

The copper(II) complexes of the type [Cu(bba)(diimine)]$(ClO_4)_2$ are involved in two types of partial intercalative mode of interactions with CT DNA, (i) *via* planar phen moiety in [Cu(bba)(phen)]$(ClO_4)_2$ (**2**, stronger) and (ii) *via* bzim moiety in [Cu(bba)(bpy)]$(ClO_4)_2$ (**1**, moderate) and [Cu(bba)(dpa)]$(ClO_4)_2$ (**3**, weak). The findings of the interaction mechanism of **1**-**3** with BSA are as follows: (a) strong quencher and interact with BSA through static quenching procedure; (b) the binding reaction is spontaneous; (c) hydrophobic interactions play a major role in the reaction; (d) affects the conformation of tryptophan residues micro-region and (e) the energy transfer occurs with high probability. These results support the fact that the Cu(II) complexes can bind to BSA and transport in the body. Further, the DNA binding, DNA cleavage and *in vitro* cytotoxicity studies show that the binding propensity, cleavage ability, and cell killing activity follow the order **2**>**1**>**3**. Overall, these studies demonstrate that **2** is promising chemotherapeutic scaffold, with well-defined biological interactions and activity derived from the redox-active copper center.

Acknowledgments

We are grateful to the DST-FIST programme of the National College (Autonomous), Tiruchirappalli. Thanks are due to SAIF, Indian Institute of Technology Madras for X-ray crystal structure data, solution, and refinement and for recording EPR spectra. Authors thank Professor A. Ramu, School of Chemistry, Madurai Kamaraj University for CD spectral measurements.

Supporting information

Crystallographic data for the structural analysis of the copper(II) complex (**1**) have been deposited with Cambridge Crystallographic Data Center, CCDC No. 1865376. Copies of this information may be obtained free of charge from http://www.ccdc.ac.uk/const/retrieving.html or from the CCDC, 12 Union Road, Cambridge CB2 1EZ, UK (email: deposit@ccdc.cam.ac.uk). Supplementary data associated with this article can be found online in the Supporting Information section at the end of the article.

References

1. R. A. Alderden, M. D. Hall, and T. W. Hambley, J. Chem. Educ. **83**, 728 (2006). https://doi.org/10.1021/ed083p728
2. Y. W. Jung and S. J. Lippard, Chem. Rev. **107**, 1387 (2007). https://doi.org/10.1021/cr068207j
3. S. Sangeetha and M. Murali, Inorg. Chem. Commun. **59**, 46 (2015). https://doi.org/10.1016/j.inoche.2015.06.032
4. S. Sangeetha and M. Murali, Int. J. Biol. Macromol. **107**, 2501 (2018). https://doi.org/10.1016/j.ijbiomac.2017.10.131
5. A. Nori and J. Kopecek, Adv. Drug Delivery Rev. **57**, 609 (2005). https://doi.org/10.1016/j.addr.2004.10.006

6. Y. Xie, G. G. Miller, S. A. Cubitt, K. J. Soderlind, M. J. Allalunis-Turner, and J. W. Lown, Anti-Cancer Drug Des. **12**, 169 (1997).
7. M. Shi, K. Ho, A. Keating, and M. S. Shoichet, Adv. Funct. Mater. **19**, 1689 (2009). https://doi.org/10.1002/adfm.200801271
8. W. O. Foye, Cancer Chemotherapeutic Agents (American Chemical Society, Washington DC, 1995).
9. B. Rosenberg, L. VamCamp, J. E. Trosko, and V. H. Mansour, Nature **222**, 385 (1969). https://doi.org/10.1038/222385a0
10. D. Senthil Raja, N. S. P. Bhuvanesh, and K. Natarajan, Dalton Trans. **41**, 4365 (2012). https://doi.org/10.1039/c2dt12274j
11. P. J. Bednarski, F. S. Mackay, and P. J. Sadler, Anticancer Agents Med. Chem. **7**, 75 (2007). https://doi.org/10.2174/187152007779314053
12. X. Qiao, Z. Y. Ma, C. Z. Xie, F. Xue, Y. W. Zhang, J. Y. Xu, Z. Y. Qiang, J. S. Lou, G. J. Chen, and S. P. Yan, J. Inorg. Biochem. **105**, 728 (2011). https://doi.org/10.1016/j.jinorgbio.2011.01.004
13. F. Kratz, in Metal Complexes in Cancer Chemotherapy, ed. B. K. Keppler (VCH: Weinheim, Germany, 1993) pp. 391.
14. M. J. McKeage, Drug Safety, **13**, 228 (1995). https://doi.org/10.2165/00002018-199513040-00003
15. A. A. Spasov, I. N. Yozhitsa, L. I. Bugaeva, and V. A. Anisimova, Pharm. Chem. J. **33**, 232 (1999). https://doi.org/10.1007/BF02510042
16. R. A. Bucknall and S. B. Carter, Nature **213**, 1099 (1967). https://doi.org/10.1038/2131099a0
17. F. Gumus, O. Algul, G. Eren, H. Eroglu, N. Diril, S. Gur, and A. Ozkul, Eur. J. Med. Chem. **38**, 473 (2003). https://doi.org/10.1016/S0223-5234(03)00058-8
18. M. Gocke, S. Utku, S. Gur, A. Rozkul, and F. Gumus, Eur. J. Med. Chem. **40**, 135 (2005). https://doi.org/10.1016/j.ejmech.2004.09.017
19. N. Bharti, M. T. Shailendra, G. Garza, E. Delia, C-. Vega, J. Castro-Garza, K. Saleem, F. Naqvi, M. R. Maurya, and A. Azam, Bioorg. Med. Chem. Lett. **12**, 869 (2002). https://doi.org/10.1016/S0960-894X(02)00034-3
20. V. G. Vaidyanathan and B. U. Nair, J. Inorg. Biochem. **91**, 405 (2002). https://doi.org/10.1016/S0162-0134(02)00448-8
21. J. Wang, L. Shuai, X. Xiao, Y. Zeng, Z. Li, and T. Matsumura-Ione, J. Inorg. Biochem. **99**, 883 (2005). https://doi.org/10.1016/j.jinorgbio.2004.12.018
22. F. Ssczewski, E. Dziemidowicz-Borys, P. J. Bednarski, R. Grünert, M. Gdaniec, and P. Tabin, J. Inorg. Biochem. **100**, 1389 (2006). https://doi.org/10.1016/j.jinorgbio.2006.04.002
23. B. Coyle, P. Kiusella, M. McCann, D. Devereux, R. O'Connor, M. Clynes, and K. Kavanagh, Toxicol. In Vitro **18**, 63 (2004). https://doi.org/10.1016/j.tiv.2003.08.011
24. D. Devereux, M. McCann, D. O'Shea, R. Kelly, D. Egan, C. Deegan, K. Kavanagh, V. McKee, and G. Finn, J. Inorg. Biochem. **98**, 1023 (2004). https://doi.org/10.1016/j.jinorgbio.2004.02.020
25. F. Gumus, G. Eren, L. Acik, A. Celebi, F. Ozturk, S. Yilmaz, R.I. Sagkan, S. Gur, A. Ozkul, A. Elmali, and Y. Elerman, J. Med. Chem. **52**, 1345 (2009). https://doi.org/10.1021/jm8000983
26. D. Wahnon, R. C. Hynes, and J. Chin, J. Chem. Soc. Chem. Commun. 1441 (1994). https://doi.org/10.1039/c39940001441
27. Z. Liao , D. Xiang , D. Li , F. Sheng , F. Mei , B. Luo, and L. Shen, Synth. React. Inorg. Met.-Org. Chem. **30**, 683 (2000). https://doi.org/10.1080/00945710009351791
28. SMART & SAINT Software References Manuals, version 5.0 (Bruker AXS Inc.: Madison, WI, 1998).
29. G. M. Sheldrick, SAINT 5.1 (Siemens Industrial Automation Inc.: Madison, WI, 1995).
30. SADABS, Empirical Absorption Correction Program (University of Göttingen: Ğottingen, Germany, 1997).
31. G. M. Sheldrick, SHELXTL Reference Manual, Version 5.1 (Bruker AXS: Madison, WI, 1997).

32. G. M. Sheldrick, SHELXS-97: Program for the Solution of Crystal Structure (University of Göttingen: Göttingen, Germany, 1997).
33. G. M. Sheldrick, ActaCrystallogr. **A64**, 112 (2008). https://doi.org/10.1107/S0108767307043930
34. C. Merill, D. Goldman, S. A. Sedman, and M. H. Ebert, Science **211**, 1437 (1980). https://doi.org/10.1126/science.6162199
35. A. T. Chaviara, E. E. Kioseoglou, A. A. Pantazaki, A. C. Tsipis, P. A. Karipidis, D. A. Kyriakidis, and C. A. Bolos, J. Inorg. Biochem. **102**, 1749 (2008). https://doi.org/10.1016/j.jinorgbio.2008.05.005
36. J. E. Huheey, E. A. Keiter, R. L. Keiter, and O. K. Medhu, Inorganic Chemistry, Principles of Structure and Reactivity (Pearson Education, Upper Saddle River, NJ, 2006) pp. 425-426.
37. A. W. Addison, T. N. Rao, J. Reedijk, J. van Rijn, and G. C. Verschoor, J. Chem. Soc. Dalton Trans. 1349 (1984). https://doi.org/10.1039/DT9840001349
38. G. Murphy, C. Murphy, B. Murphy, and B. J. Hathway, Dalton Trans. 2653 (1997). https://doi.org/10.1039/a702293j
39. P. T. Selvi, M. Murali, M. Palaniandavar, M. Kockerling, and G. Henkel, Inorg. Chim. Acta **340**, 139 (2002). https://doi.org/10.1016/S0020-1693(02)01091-5
40. M. Palaniandavar, T. Pandiyan, M. Lakshminarayanan, and H. Manohar, J. Chem. Soc. Dalton Trans. **3**, 455 (1995). https://doi.org/10.1039/dt9950000455
41. K. Pijus, S. Saha, R. Majumdar, R. R. Dighe, and A. R. Chakravarty, Inorg. Chem. **49**, 849 (2010). https://doi.org/10.1021/ic900701s
42. T. -H. Huang, H. Yang, G. Yang, S. -I. Zhu, and C. -L. Zhang, Inorg. Chim. Acta **455**, 1 (2017). https://doi.org/10.1016/j.ica.2016.10.012
43. T. -H. Huang, M. -H. Zhang, C. -Y. Gao, and L. -T. Wang, Inorg. Chim. Acta **408**, 91 (2013). https://doi.org/10.1016/j.ica.2013.08.024
44. A. B. P. Lever, Inorganic Electronic Spectroscopy (Elsevier, Amsterdam, 1984).
45. V. Sathya and M. Murali, Inorg. Chem. Commun. **92**, 55 (2018). https://doi.org/10.1016/j.inoche.2018.04.003
46. U. Sakaguchiand A.W. Addison, J. Chem. Soc. Dalton Trans. 600 (1979). https://doi.org/10.1039/dt9790000600
47. M. Palaniandavar, I. Somasundaram, M. Lakshminarayanan, and H. Manohar, Dalton Trans. 1333 (1996). https://doi.org/10.1039/dt9960001333
48. M. Murali, M. Palaniandavar and T. Pandiyan, Inorg. Chim. Acta **224**, 19 (1994). https://doi.org/10.1016/0020-1693(94)04009-5
49. C. Rajarajeswari, R. Loganathan, M. Palaniandavar, E. Suresh, A. Riyasdeen, and M. A. Akbarsha, Dalton Trans. **42**, 8347 (2013). https://doi.org/10.1039/c3dt32992e
50. E. Turkkan, U. Sayin, N. Erbilen, S. Pehlivanoglu, G. Erdogan, H. U. Tasdemir, A. O. Saf, L. Guler, and E. G. Akgemci, J. Organomet. Chem. **831**, 23 (2017). https://doi.org/10.1016/j.jorganchem.2016.12.020
51. B. J. Hathaway, Copper in: Comprehensive Coordination Chemistry (Pergamon Press, Oxford, 1987) **5**, pp. 533-774.
52. R. Balamurugan, M. Palaniandavar, H. Stoeckli-Evans, and M. Neuburger, Inorg. Chim. Acta **359**, 1103 (2006). https://doi.org/10.1016/j.ica.2005.09.062
53. B. D. Wang, Z. D. Y. Yang and T. R. Li, Bioorg. Med. Chem. **14**, 6012 (2006). https://doi.org/10.1016/j.bmc.2006.05.015
54. J. B. Le Pecq and C. Paoletti, J. Mol. Biol. **27**, 87 (1967). https://doi.org/10.1016/0022-2836(67)90353-1
55. S. Ramakrishnan, V. Rajendiran, M. Palaniandavar, V. S. Periasamy, B. S. Srinag, H. Krishnamurthy, and M. A. Akbarsha, Inorg. Chem. **48**, 1309 (2009). https://doi.org/10.1021/ic801144x
56. Y. B. Zeng, N. Yang, W. S. Liu, and N. Tang, J. Inorg. Biochem. **97**, 258 (2003). https://doi.org/10.1016/S0162-0134(03)00313-1

57. T. Hirohama, Y. Kuranuki, E. Ebina, T. Sugizaki, H. Arii, M. Chikira, P. T. Selvi, and M. Palaniandavar, J. Inorg.Biochem. **99**, 1205 (2005). https://doi.org/10.1016/j.jinorgbio.2005.02.020
58. M. R. Eftink and C. A. Ghiron, Anal. Biochem. **114**, 199 (1981). https://doi.org/10.1016/0003-2697(81)90474-7
59. X. Zhao, R. Liu, Z. Chi, Y. Teng, and P. Qin, J. Phys. Chem. B **114**, 5625 (2010). https://doi.org/10.1021/jp100903x
60. W. He, Y. Li, C. Xue, Z. Hu, X. Chen, and F. Sheng, Bioorg. Med. Chem. **13**, 1837 (2005). https://doi.org/10.1016/j.bmc.2004.11.038
61. A. Sulkowska, J. Równicka, B. Bojko, and W. Sułkowski, J. Mol. Struct. **651**, 133 (2003). https://doi.org/10.1016/S0022-2860(02)00642-7
62. P. D. Ross and S. Subramanian, Biochemistry **20**, 3096 (1981). https://doi.org/10.1021/bi00514a017
63. C. N. Lunardi, A. C. Tedesco, T. L. Kurth, and I. M. Brinn, Photochem. Photobiol. Sci. **2**, 954 (2003). https://doi.org/10.1039/B301789C
64. J. N. Miller, Proc. Anal. Div. Chem. Soc. **16**, 203 (1979). https://doi.org/10.1039/ad9791600199
65. T. Förster and O. Sinanoglu, Modern Quantum Chemistry (Acdemic Press, New York, 1966) **3**.
66. Y. Wang, Y. Wei, and C. Dong, J. Photochem. Photobiol. **177**, 6 (2006). https://doi.org/10.1016/j.jphotochem.2005.04.040
67. B. Saha, M. M. Islam, S. Paul, S. Samanta, S. Ray, C. R. Santra, S. R. Choudhury, B. Dey, A. Das, S. Ghosh, S. Mukhopadhyay, G. S. Kumar, and P. Karmakar, J. Phys. Chem. B **114**, 5851 (2010). https://doi.org/10.1021/jp909127a
68. J. Tan, B. Wang, and L. Zhu, J. Biol. Inorg. Chem. **14**, 727 (2009). https://doi.org/10.1007/s00775-009-0486-8
69. M. G. Pandian, R. Loganathan, S. Ramakrishnan, E. Suresh, A. Riyasdeen, M. A. Akbarsha, and M. Palaniandavar, Polyhedron **52**, 924 (2013). https://doi.org/10.1016/j.poly.2012.07.021
70. Y. Gou, J. Li, B. Fan, B. Xu, M. Zhou, and F. Yang, Eur. J. Med. Chem. **134**, 207 (2017). https://doi.org/10.1016/j.ejmech.2017.04.026